Chinese Journal of Chemical Engineering 89 (2026) 93–101

Contents lists available at ScienceDirect

Chinese Journal of Chemical Engineering

journal homepage: www.elsevier.com/locate/CJChE

Full Length Article

Adsorption of flubendiamide (pesticide) onto chitosan-modified magnetic biochar in environmental remediation

Hong-Hue Thi Nguyen [1], Yong-Ho Choi [2], Yong-Hoon Jeong [3], Jong-Guk Kim [4,*], Dong-Heui Kwak [1,3,*]

[1] *Department of Bioactive Material Sciences, Jeonbuk National University, Jeonju 54896, Korea*
[2] *Innovative Research and Education Center for Integrated Bioactive Materials, Jeonju 54896, Korea*
[3] *Department of Bio-Convergence Science, Jeonbuk National University, Jeongeup 56212, Korea*
[4] *Division of Civil/Environmental/Mineral Resources and Energy Engineering (Department of Environmental Engineering), Jeonbuk National University, Jeonju 54896, Republic of Korea*

ARTICLE INFO

Article history:
Received 6 April 2025
Received in revised form
2 September 2025
Accepted 3 September 2025
Available online 26 September 2025

Keywords:
Adsorption
Biomass
Chitosan
Modified biochar
Pesticide
Waste treatment

ABSTRACT

Flubendiamide is a commonly used pesticide with low water solubility and a high organic carbon sorption constant, causing it to adhere to soil particles and negatively impact soil ecosystems. First, chili plant stems, typically discarded after the harvest season, represent an abundant local biomass resource with significant potential for utilization, and were converted into biochar through pyrolysis. Here, we describe the synthesis of biochar modified with iron and chitosan to increase the diversity of functions and surface functional groups of biochar. The resulting chitosan-modified magnetic biochar (CMBC) presents a full range of functional groups of chitosan and iron oxide as shown by Fourier-transform infrared spectroscopy. The correlation between flubendiamide concentration and the dose of biochar on adsorption was explored. The flubendiamide adsorption efficiency of CMBC (1% mass ratio of soil) reached 68.03% in 90 min. The highest adsorption capacity achieved was 0.95 $mg \cdot g^{-1}$. The flubendiamide adsorption mechanism by CMBC can be described with a pseudo-second-order kinetic model. The experiment data closely fit a Freundlich isotherm model ($R^2 = 0.998$), and the low residual sum of squares values demonstrate the high model applicability. In this study, we present a comprehensive overview of pesticides, alongside kinetic and isotherm model studies of flubendiamide adsorption by CMBC. We emphasize the potential of modified biochar to enhance environmental remediation applications.

1. Introduction

Pesticides play a crucial role in modern agriculture, as they help protect crops from harmful pests, leading to increased productivity [1,2]. However, pesticides are engineered to have stable molecular structures to resist the attack of many types of pests on crops. Pesticides with stable molecular structures often exhibit high toxicity due to their resistance to degradation and strong interaction with biological targets. As highlighted in structure-toxicity relationship studies, features such as molecular symmetry, polarity, and the nature of substituents directly influence how pesticides persist in the environment, accumulate in organisms, and prolong toxic effects [2]. Based on their intended use and target, pesticides can be classified as insecticides, herbicides, or fungicides [3]. However, because pests may develop resistance to pesticides after prolonged exposure, there is a demand for a broader range of pesticides with greater toxicity and strength. One consequence of this situation is the presence of pesticide residues in the environment [4], which can alter the structure and properties of soil, increasing exposure to diverse soil ecosystems [5]. Moreover, pesticides enter the aquatic environment through runoff from agricultural areas and threaten aquatic biodiversity. These chemicals present significant risks to human health through direct and indirect exposure *via* food consumption [6–9].

* Corresponding authors. These authors contributed equally as corresponding authors.
E-mail addresses: kjongguk@jbnu.ac.kr (J.-G. Kim), kwak124@jbnu.ac.kr (D.-H. Kwak).

https://doi.org/10.1016/j.cjche.2025.09.005

Flubendiamide (N^1-[4-(1,1,1,2,3,3,3-heptafluoropropan-2-yl)-2-methylphenyl]-3-iodo-N^2-[1-(methanesulfonyl)-2-methylpropan-2-yl]benzene-1,2-dicarboxamide) is a synthetic pesticide, commonly applied to control pests on rice, vegetables, and fruit trees. It activates calcium channels that release calcium ions stored in the endoplasmic reticulum of cells in insect bodies, causing paralysis and death [10,11]. Some physicochemical properties of flubendiamide are presented in Table 1 [11,12].

Flubendiamide has poor water solubility and low vapor pressure, but it is persistent in the environment and accumulates in soil. It has a hydrophobic nature and a high partition coefficient ($\lg P_{o/w}$) and tends to be more soluble in nonpolar organic solvents than in water. A high organic carbon sorption constant (K_{oc}) allows it to bind easily to soil particles, causing negative impacts on soil ecosystems. Flubendiamide has been shown to degrade more rapidly at acidic pH levels than at basic pH levels, and the slowest degradation in water is reported at neutral pH levels. Specifically, in one experiment over 120 days, flubendiamide showed the highest dissipation rate at pH 4.0, with 22.3% loss, followed by 21.0% at pH 9.2 and 18.5% at pH 7.0. Correspondingly, the calculated half-life values based on single-phase first-order kinetics were shortest under acidic conditions (250.8 days), slightly longer under basic conditions (273.6 days), and longest at neutral pH (301 days). The degradation is attributed to the hydrolysis of the two amide linkages in the molecular structure. The amide bond in flubendiamide can be hydrolyzed (broken) by water. In an acidic environment, the carbonyl group of the amide is easily protonated, promoting faster hydrolysis. Conversely, in an alkaline environment, the hydroxide ion (OH^-) can directly attack the carbon of the amide bond. Therefore, the higher degradation rate at acidic and alkaline pH is due to conditions promoting amide bond hydrolysis, while at neutral pH, this mechanism is less efficient [13,14]. Besides, some studies have shown that flubendiamide can be toxic to non-target organisms, such as earthworms and beneficial microorganisms, at high concentrations [10]. According to the Flubendiamide Market Report 2025, the global flubendiamide market is projected to grow steadily from a market size of $499.1 million in 2025 to $714.24 million by 2033. This growth reflects a compound annual growth rate of 4.582%, indicating a consistent rise in demand across various crop applications such as cereals, fruits, vegetables, and oilseeds. Thus, it is essential to minimize flubendiamide accumulation in the soil environment by implementing sustainable strategies.

Biochar is widely recognized as a green adsorbent, as it undergoes carbonization in an oxygen-free environment, transforming organic materials into valuable and sustainable products [15–17]. Biochar has a porous structure, a large surface area, and is highly stable. It is often applied to adsorb and reduce environmental pollutants [18–20]. Attempts have been made to create more efficient types of biochar, enhance its capacity to adsorb pollutants, improve water retention, and increase its effectiveness in environmental remediation.

Biochar can be converted into magnetic biochar (MBC) when modified with inexpensive, common, green magnetic particles such as zero-valent iron (Fe^0) and iron oxides (Fe_2O_3 or Fe_3O_4). MBC not only demonstrates an adsorption capacity due to the advantageous characteristics of conventional biochar but also facilitates its separation from the environment after treatment, addressing a limitation in its environmental application [21–24]. Chitosan is an eco-friendly material derived from natural sources, such as shells of crustaceans [25]. Due to its multiple amine ($-NH_2$) and hydroxyl ($-OH$) groups, chitosan can form hydrogen bonds, ionic bonds, and electrostatic interactions with pollutants [26] and can be used to create chitosan-modified magnetic biochar (CMBC) [27,28]. Chitosan introduces an additional diversity of functional groups that chemically adsorb pollutant molecules onto the MBC matrix. MBC offers a robust, porous framework that ensures effective dispersion of chitosan.

To the best of our knowledge, no studies on the adsorption capacity of CMBC for pesticides have been conducted. In this study, we used the stems of a common agricultural crop in Jeonbuk-do, the chili plant. We then assessed the effectiveness of CMBC to remove pesticide residues from agricultural soil.

2. Materials and Methods

2.1. Chemicals

A water purification system (EXL-3 Pure, Vivagen, Korea) was used to produce deionized (DI) water. Iron(II) chloride tetrahydrate ($FeCl_2 \cdot 4H_2O$, ≥99.0%), iron(III) chloride hexahydrate ($FeCl_3 \cdot 6H_2O$, ≥98.0%), acetic acid (CH_3COOH, ≥99%), low-molecular-weight chitosan, and high-purity flubendiamide ($C_{23}H_{22}F_7IN_2O_4S$, ≥98.0%) were purchased from Sigma Aldrich (Merck, Germany). Sodium hydroxide (NaOH, ≥99.0%) and acetonitrile (CH_3CN, ≥99.5%) were from Deajung, Republic of Korea. All chemicals employed in these experiments were of analytical grade.

2.2. Soil sample

In a study by Suh *et al.* [29] in 300 soil sites in Korea, 42 types of pesticides were detected. In agricultural soil monitoring, flubendiamide was among the top five pesticides detected at concentrations between 0.023 and 0.499 $mg \cdot kg^{-1}$. Flubendiamide ranked among the top six most frequently detected pesticides in agricultural soils across various orchard cropping systems, including apple, peach, persimmon, and grape cultivation. According to the environmental risk assessment conducted for orchard soils, flubendiamide exhibited acute and chronic toxicity to soil organisms under typical field conditions. The quantitative distribution of pesticide residues in Jeonbuk-do was 0.05–0.1 $mg \cdot kg^{-1}$ soil weight, emphasizing the pesticide-residue status and the risk of long-term soil pollution [29].

Three agricultural soils were selected to be contaminated with flubendiamide for laboratory-scale experiments. Soil samples were collected from two sites (0.1–0.25 mg per kg soil) and one site (0.25–1.0 mg per kg soil) in an agricultural field in Gimje, Jeollabuk-do, South Korea. The samples were dried in an oven at 60 °C, then crushed and sieved through a 2 mm mesh to remove larger stones and plant residues, rewashed with DI water, dried again in an oven at 60 °C [30], and stored for further use.

Table 1
Physico-chemical properties of flubendiamide.

Pesticide	Type	Molecular weight/$g \cdot mol^{-1}$	Solubility (in 20 °C)/$g \cdot L^{-1}$	Partition coefficient (in 24.9 ± 0.1), $\lg(P_{o/w})$	Organic carbon sorption constant, K_{oc}	Vapor pressure (in 25 °C)/mPa
Flubendiamide	Insecticide	682.39	29.9×10^{-6}	4.20	600–900	1×10^{-1}

2.3. Characterization of adsorbents

The synthesis process was performed following the steps described in Ref. [28]. Biomass was derived from chili plant stems harvested from an agricultural field in Gimje, Jeonbuk-do. Chili stems are discarded after harvesting. We collected this discarded material and brought it to the laboratory to serve as biomass. The biomass was washed with tap water and DI water, chopped into pieces approximately 2 cm in diameter, and dried overnight at 105 °C in a laboratory oven. The chili plant biomass was pyrolyzed in a programmable tube furnace pyrolysis reactor (SH-FU-80STG-WG, SH SCIENTIFIC, USA) at a heating rate of 10 °C·min^{-1} until the temperature reached 500 °C. Pyrolysis was maintained at this temperature for 4 h with a continuous flow of nitrogen (N_2) gas. After completion, the reactor was allowed to cool to room temperature. The chili stem-originated biochar was removed and stored for later use.

Initially, 5 g of biochar was placed in a glass beaker. An iron ion solution prepared from 0.86 g of $FeCl_2 \cdot 4H_2O$ and 2.36 g of $FeCl_3 \cdot 6H_2O$ was added and completely dissolved in 50 ml of DI water under stirring, ensuring the solution fully covered the biochar. In impregnation, the mixture was stirred for 12 h (room temperature) to achieve a uniform distribution of iron ions on the biochar surface. Then, the mixture was heated to approximately 80 °C, after which 50 ml of 1 mol ·L^{-1} NaOH solution was added gradually to the iron ion-biochar mixture under constant stirring at 80 °C for 1–2 h to facilitate the complete precipitation of iron ions. The resulting precipitate was filtered and washed multiple times with DI water to eliminate residual ions and impurities. The final product was dried at 105 °C to obtain the MBC.

The synthesis of CMBC began with dissolving chitosan powder in a 1% (volume ratio) aqueous acetic acid solution at a concentration of 1% (mass to volume ratio) to form a chitosan solution. Next, 1 g of MBC was added to 20 ml of this solution and mixed rapidly for 1 h at room temperature. To induce precipitation, 20 ml of 1 mol· L^{-1} NaOH solution was gradually introduced dropwise while maintaining continuous stirring for another hour. When NaOH was added to the solution, the pH of the solution increased, and the chitosan changed from a soluble to an insoluble form, precipitating onto the MBC surface [31]. Finally, the mixture was filtered, washed repeatedly with DI water to remove NaOH, and oven-dried at 60 °C.

The characteristics of the adsorbents were explored using various techniques. Surface morphology was examined using a scanning electron microscope (SEM, Hitachi S-4700, Japan), providing detailed insights into the structural features of the CMBC surfaces. Fourier-transform infrared spectroscopy (FT-IR) using an FT/IR-8X apparatus (JASCO, Japan) was used to identify the functional groups and overall molecular structure, revealing the chemical composition and potential interactions of the CMBC. Additionally, nitrogen adsorption and desorption measurements conducted at −196 °C (using a Belsorp mini II, BEL, Japan) determined the specific surface area (S_{BET}) using the Brunauer–Emmett–Teller (BET) method. The total pore volume (V_{BJH}) and pore area (a_{pore}) were calculated using the Barrett–Joyner–Halenda (BJH) method, providing a comprehensive understanding of the pore characteristics essential for adsorption. The elemental composition and chemical states of CMBC were analyzed with X-ray photoelectron spectroscopy (XPS), using Axis Supra+ (Kratos Analytical Ltd., Japan). Zeta potential measurements of CMBC particles were carried out using dynamic light scattering with a ZEN3600 analyzer (Malvern Instruments, UK).

2.4. Adsorption experiments

We conducted a series of experiments to investigate the adsorption behavior of CMBC on flubendiamide and evaluate its adsorption efficiency.

First, flubendiamide was prepared in DI water. Flubendiamide is a hydrophobic compound and has low solubility in water, necessitating prior dissolution in acetonitrile, which is a moderately polar organic solvent widely used in chromatographic analyses [12,32]. In our experiments, flubendiamide was dissolved in acetonitrile at a volumetric ratio of 10% of the final solution. To make 100 ml of flubendiamide solution, 1, 3, and 5 mg of pure flubendiamide powder were dissolved in 10 ml of acetonitrile for each solution, respectively. Dissolution was carried out in a volumetric flask, ensuring precise control of the solution volume.

Following complete dissolution in acetonitrile, DI water was gradually introduced dropwise from a burette into the volumetric flask under mild heating (approximately 70 °C) and magnetic stirring to maintain homogeneity. However, when DI water was added, the solubility of flubendiamide was changed, and it partially precipitated. Once the desired solution volume was achieved, the mixture was poured through filter paper to remove insoluble impurities or precipitates and ensure solution homogeneity. This process is illustrated in Fig. 1.

After filtering off some of the precipitated flubendiamide, the final flubendiamide concentration in solution (pH 5.6) was determined using high-performance liquid chromatography (HPLC), a sensitive and precise analytical technique used extensively to analyze pesticide residue and environmental chemistry. The analytical conditions for determining the flubendiamide concentration involved the use of an LC-40 HPLC system (Shimadzu, Japan) equipped with a photodiode array detector. Separation was achieved using a Phenomenex Bondclone C18 column (10 μm, 250 mm × 3.9 mm) with a mobile phase of water and acetonitrile

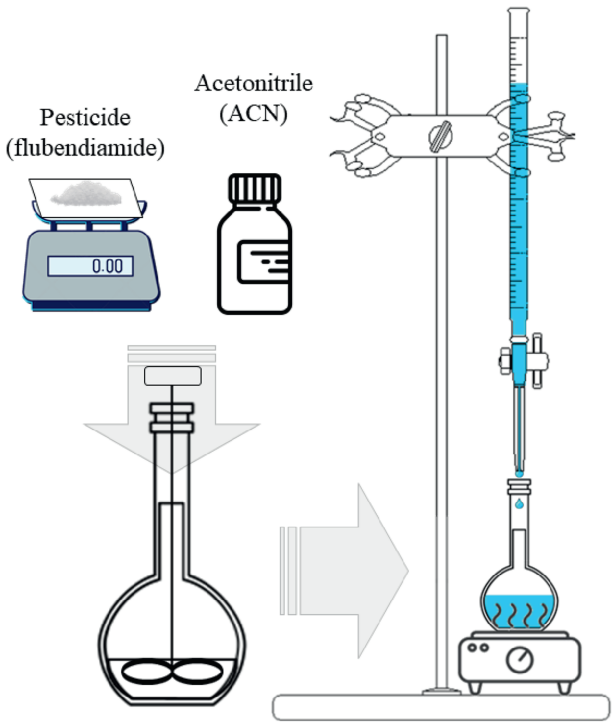

Fig. 1. Preparation of flubendiamide solution.

in a 40:60 vol ratio, delivered at a flow rate of 1.0 ml min^{-1}. The column oven temperature was maintained at 30 °C to ensure stable separation conditions. The injection volume was 10 μl. Besides, in this study, we conducted preliminary experiments to test the pH-dependent behavior of CMBC under different pH conditions (pH 2 and pH 10). However, in these experiments, the flubendiamide concentration in the supernatants after interaction was beyond the detection limit of HPLC, possibly due to the pH environment changing the surface charge of the biochar or due to background interference.

Specific amounts of CMBC (0.02, 0.05, and 0.1 g, equivalent to 1%, 2.5%, and 5% by mass of soil, respectively) were added to 50 ml conical tubes containing 2.00 g of soil. Next, we added 20 ml of flubendiamide solution with a known concentration to each tube. The centrifuge tubes were then shaken in a shaker at 150 $r \cdot min^{-1}$ at room temperature to ensure contact among the components. After specific shaking times (10, 20, 30, 60, 90, or 120 min), the sample tubes were centrifuged for 5 min and filtered through a 0.45 μm membrane filter to remove insoluble particles from the supernatants. The concentration of the pesticide in the supernatant solution was analyzed by HPLC, and the flubendiamide adsorption kinetics of CMBC were studied. The adsorption efficiency of biochar and MBC was evaluated using the following equation:

$$\text{Adsorption efficiency} = \frac{C_0 - C_t}{C_0} \times 100\%$$

where C_0 ($mg \cdot L^{-1}$) is the initial pesticide concentration, and C_t ($mg \cdot L^{-1}$) is the concentration of pesticides at time t (min). Flubendiamide at various concentrations (0.883, 1.129, 1.257, and 1.323 $mg \cdot L^{-1}$) interacted with 0.02 g of CMBC in a similar experimental method. Each experimental condition was repeated twice to ensure reliability. Here, the experimental data were studied using isotherm adsorption.

2.5. Analytical methods

The adsorption results were analyzed using adsorption kinetics and isotherm studies as shown in Table 2. Adsorption kinetic studies analyze the speed of adsorbate removal from a solution and interaction with adsorbent surfaces. A pseudo-first-order (PFO) kinetic model typically assumes that the adsorption rate decreases proportionally as the adsorption capacity increases, establishing a linear relationship between adsorption capacity and time-dependent change. In contrast, a pseudo-second-order (PSO) kinetic model assumes the rate-limiting step to be an interaction between the adsorbent and adsorbate. Such a model is commonly used for adsorption driven by chemical interactions, such as covalent bonding, ion exchange, or surface complexation, where the adsorption rate depends on the square of the available adsorption sites [33–35]. PFO and PSO kinetic equations are shown in Table 2.

Adsorption isotherm studies typically focus on adsorbate distribution between the solid phase (adsorbent) and the liquid phase at equilibrium. The Langmuir isotherm model is best suited for monolayer adsorption on a homogeneous surface with a finite number of identical adsorption sites, assuming no interactions between adsorbed molecules. This model assumes that adsorption is uniform until a complete monolayer forms, after which no further adsorption occurs. The Freundlich isotherm model is more appropriate for multilayer adsorption on heterogeneous surfaces with varying adsorption energies. It accounts for surface irregularities and different binding affinities and is particularly useful for describing non-ideal adsorption. Here, the model's applicability was evaluated by calculating the residual sum of squares (RSS) content (Table 2) [28,35].

3. Results and Discussion

3.1. Characterization of CMBC

3.1.1. Surface morphology

The morphological properties of CMBC are depicted in Fig. 2. An SEM image reveals a clear porous structure. The pores diverse variations in sizes and shapes, resemble tunnels on the CMBC surface. In addition, the rough inner surfaces of the pores contributes to the high overall surface area of CMBC. Small particles, which may be iron oxide crystals and debris, adhere to the surface of the material during the synthesis of CMBC, but they are not concentrated into clusters and so do not block the pores and affect the adsorption performance of CMBC.

3.1.2. Adsorption–desorption isotherm analysis results

Nitrogen adsorption–desorption isotherms for CMBC are depicted in Fig. 3. Analysis showed that the model exhibited a type IV isotherm with hysteresis loops. According to the International

Table 2
Adsorption kinetics and isotherm equations.

Types		Equation	Linear form	Parameter	
Adsorption kinetics	PFO	$\frac{dq_t}{dt} = k_1(q_e - q_t)$	$\ln\left(\frac{q_e}{q_t}\right) = \ln q_e - k_1 t$	q_e/$mg \cdot g^{-1}$	Equilibrium adsorption capacity
				q_t/$mg \cdot g^{-1}$	Adsorption capacity at time t
				k_1/min^{-1}	Rate constant of PFO
	PSO	$\frac{dq_t}{dt} = k_2(q_e - q_t)^2$	$\frac{t}{q_t} = \frac{1}{k_2 q_e^2} + \frac{t}{q_e}$	k_2/$g \cdot mg^{-1} \cdot min^{-1}$	Rate constant of PSO
Adsorption isotherms	Langmuir isotherms	$q_e = \frac{q_{max} K_L C_e}{1 + K_L C_e}$	$\frac{C_e}{q_e} = \left(\frac{1}{q_{max}}\right) C_e + \left(\frac{1}{q_{max} K_L}\right)$	q_e/$mg \cdot g^{-1}$	Amount of flubendiamide adsorbed per unit weight of adsorbent
				C_e/$mg \cdot L^{-1}$	Equilibrium concentration of the solute bulk solution
				q_{max}/$mg \cdot g^{-1}$	Maximum adsorption capacity
				K_L/$L \cdot mg^{-1}$	Langmuir isotherm constant
	Freundlich isotherms	$q_e = K_F C_e^{1/n}$	$\lg q_e = \frac{1}{n} \ln C_e + \ln K_F$	K_F/$(mg \cdot g^{-1}) \cdot (L \cdot mg^{-1})^{1/n}$	Freundlich isotherm constant
				$1/n$	Heterogeneity factor of the Freundlich model
	RSS	$RSS = \sum (q_e^{exp} - q_e^{pred})^2$		q_e^{exp}/$mg \cdot g^{-1}$	Adsorption capacity from experiment
				q_e^{pred}/$mg \cdot g^{-1}$	Predicted adsorption capacity

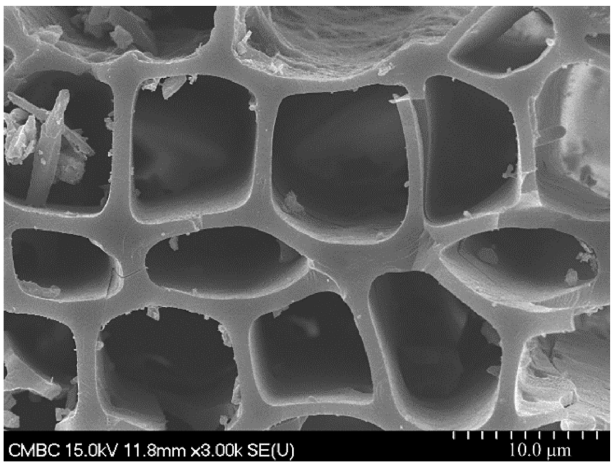

Fig. 2. SEM images of CMBC.

Union of Pure and Applied Chemistry (IUPAC) classification, a type IV isotherm is characteristic of mesoporous materials, which play a crucial role in adsorption applications by balancing surface area and diffusion pathways for adsorbates. The adsorption isotherm increases slightly in the relative pressure range of 0–0.4 P/P_0, indicating monolayer adsorption on the material surface. This is followed by a gradual increase in the adsorption curve due to the saturation of monolayer adsorption, followed by polymolecular adsorption. When the relative pressure is in the range of 0.4–0.9 P/P_0, the desorption branch is significantly higher than the adsorption branch due to the occurrence of capillary condensation. This phenomenon results in a hysteresis loop, indicating condensation within mesopores, with gas molecules progressively filling medium and large pores. When the relative pressure reached 0.9 to 1.0 P/P_0, both the adsorption and desorption branches showed a sudden increase. Finally, these branches intersected, indicating that the desorption process was complete and the large pores were full [36,37].

The pore-size distribution of CMBC is shown in Fig. 3, with pore sizes of CMBC ranging from 2 to 50 nm, making it a mesoporous material according to IUPAC standards. This mesoporous nature offers a high surface-to-volume ratio, increasing the number of interaction sites between the adsorbent and the target species. Moreover, mesoporous structures can enhance molecular transport efficiency by mitigating diffusion limitations commonly associated with microporous materials. This makes them particularly effective for the removal of organic pollutants [28,38].

The specific surface area, as calculated by the BET method, produces an S_{BET} of 16.00 $m^2 \cdot g^{-1}$. A modified surface with iron and chitosan can enhance the functional groups, contributing to its chemical reactivity [39]. Calculation using the BJH method gives a V_{BJH} of 0.0567 $cm^3 \cdot g^{-1}$ and a_{pore} of 24.213 $m^2 \cdot g^{-1}$, reflecting a relatively high pore density and facilitating the diffusion and immobilization of adsorbent.

The zeta potential of the CMBC particles was measured to be approximately −11 mV at the reaction pH 5.6, indicating a moderately negative surface charge. This surface characteristic is favorable for the adsorption of a neutral and hydrophobic flubendiamide, as it promotes hydrophobic interactions and possible electrostatic bonds between the biochar surface and the aromatic structure of flubendiamide. The negative zeta potential also suggests good colloidal stability, the ensuring effective dispersion of CMBC during the adsorption process.

3.1.3. FT-IR analysis results

The FT-IR spectra of CMBC were significantly different from those of biochar and chitosan, as shown in Fig. 4. The peak at 3500 cm^{-1} corresponds to O—H stretching, and the peaks at 3286 and 3350 cm^{-1} of N—H stretching were broadened and enhanced compared with those of biochar, reflecting the presence of chitosan on the biochar surface [27]. The increase in peaks at 1585 cm^{-1} (C═O stretching) and 1530 cm^{-1} (N—H bending and C—N stretching) confirmed the presence of amine groups (—NH_2) in chitosan, as well as the change in the aromatic structure of biochar [40]. The influence of chitosan on the functional groups on the biochar surface was also demonstrated by the enhancement of the peak at 1370 cm^{-1} (C—N stretching). The changes in peak intensity at 1066 and 1020 cm^{-1} of C—O—C stretching represent the combination of biochar and chitosan on CMBC. At the same time, the decrease in intensity of peaks at 876 and 823 cm^{-1} (aromatic C—H bending structure of biochar) after modification may indicate chitosan coating of the biochar surface. In particular, a clear peak at 550 cm^{-1} appeared, indicating Fe—O vibration and confirming the presence of iron in the material [41,42]. These changes in the FT-IR spectra of biochar, chitosan, and CMBC indicate the

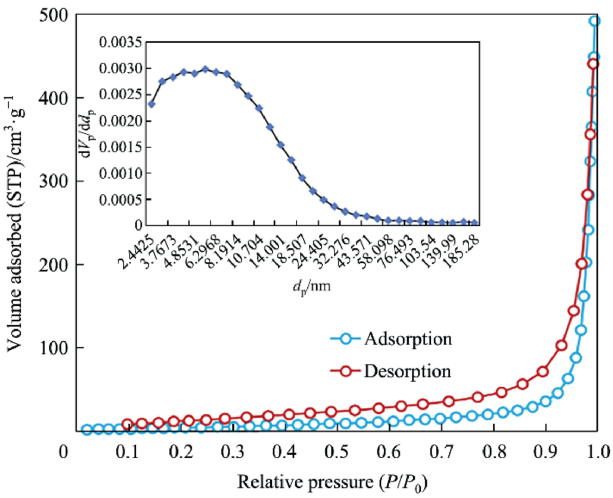

Fig. 3. Nitrogen adsorption–desorption isotherms and pore-size distribution of CMBC.

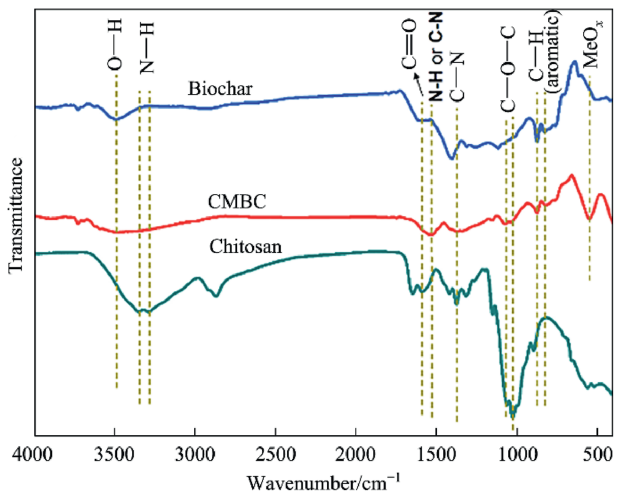

Fig. 4. FT-IR spectra of CMBC and comparison.

successful deposition of chitosan and iron onto the biochar surface, creating materials with diversified functional groups.

3.1.4. XPS analysis results

The XPS surface analysis results of the CMBC adsorbent are presented in Fig. 5, alongside the spectra of pristine biochar and MBC before chitosan modification. The C 1s and N 1s signals exhibited a decreasing trend in intensity from biochar to MBC, with a more pronounced reduction observed in the CMBC sample. This reflects the alterations in carbon and nitrogen content resulting from the surface modification, consistent with the trend observed in the FT-IR analysis. Notably, the surface Fe content was significantly higher in the MBC sample compared to the original biochar, confirming the effectiveness of the iron impregnation process. However, following chitosan modification, the Fe signal intensity on the CMBC surface decreased, likely due to partial surface coverage by the chitosan polymer, which may have attenuated the Fe signal during XPS detection.

3.2. Adsorption capacity and adsorption kinetics

The adsorption efficiency of different doses of CMBC over 90 min of interaction at the same flubendiamide concentration was investigated (Fig. 6). The adsorption kinetics were analyzed using PFO and PSO models, and the calculated parameter values are presented in Table 3.

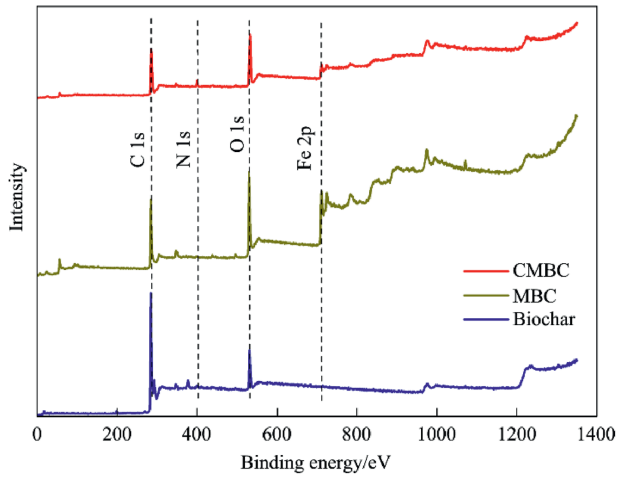

Fig. 5. XPS spectra of CMBC and comparison.

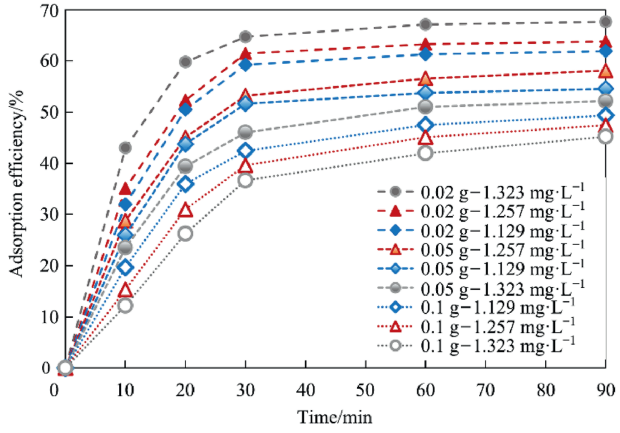

Fig. 6. Flubendiamide adsorption efficiency of CMBC.

3.2.1. Effect of CMBC dose at a fixed flubendiamide concentration

Among the parameters affecting adsorption, the dose of the adsorbent plays a crucial role as it directly influences the equilibrium between the adsorbent and adsorbate within the system [43].

At a flubendiamide concentration of 1.129 mg·L^{-1}, when the CMBC dose was increased from 0.02 g to 0.05 g and 0.1 g, the adsorption efficiency decreased by 12.04%. The coefficient of determination (R^2) was higher for the PSO model ($R^2 = 0.989–0.994$) than the PFO model ($R^2 = 0.834–0.975$) across all doses of CMBC. This indicates that the PSO model provided superior predictive accuracy in describing the chemical adsorption interactions compared to the PFO model, which primarily represents physical adsorption. In the PSO model, k_2 increased significantly by 1%, 2.5%, and 5% CMBC (mass ratio of soil). This shows an increasing trend in adsorption due to the increasing number of adsorption sites, resulting in a more rapid equilibrium. In contrast, the q_e value decreased dramatically as the dose of CMBC was increased. This increase in the number of adsorbent molecules resulted in wider dispersion to various locations, leading to competition for available binding sites, decreasing the adsorption capacity per unit mass of the adsorbent [33,44].

At 1.257 mg L^{-1} of flubendiamide, the adsorption efficiency by CMBC decreased by 15.71% as the CMBC dose increased from 0.02 g to 0.1 g. This adsorption was well described by the PSO model; however, when the CMBC dose reached 0.1 g, the adsorption process was better represented by the PFO model ($R^2 = 0.985$ of PFO model is higher than $R^2 = 0.974$ of PSO). This implies a shift in the adsorption mechanism from chemical interactions to physical surface adsorption. The value of k_1 in the PFO model decreased gradually, while that in the PSO model increased due to the increase of adsorption sites and then decreased slightly when the adsorbent had filled many of the pores, leading to competition for adsorption sites. As not all adsorbent particles were accessible for cross-linking or ion exchange, the overall adsorption rate was limited, similar to the downward trend in q_e values observed in the PFO model. The q_e values in both kinetic models decreased, though the change was gradual with the PFO model but sharp with the PSO model [44–46].

Similarly, at a flubendiamide concentration of 1.323 mg L^{-1}, the adsorption efficiency significantly decreased (22.53%) as the CMBC dose increased. When the CMBC dose reached 0.1 g, the adsorption trend shifted gradually from being predominantly driven by chemical interactions to physical diffusion, demonstrated by the better fit of the PFO model than the PSO model ($R^2 = 0.970$ of PFO > $R^2 = 0.949$ of PSO). The k_1 and k_2 values increased at 0.05 g of CMBC but decreased at a higher CMBC dose of 0.1 g. The q_e values followed similar trends to those observed for 1.257 mg·L^{-1} flubendiamide, which can be attributed to the increase and competition between adsorption sites.

3.2.2. Effect of flubendiamide concentration at a fixed dose of biochar

The initial concentration of the adsorbate provides a significant driving force to overcome mass transfer resistance and reach the adsorbent [47,48].

As the flubendiamide influent concentration increased from 1.129 to 1.323 mg·L^{-1}, the natural adsorption of the flubendiamide to the soil (in the absence of CMBC) was observed and confirmed under constant experimental conditions. After the interaction, the amount of flubendiamide retained in the soil increased slightly, with the removal efficiency by approximately 3.6% to 4.6% at higher concentrations. This suggests that flubendiamide has a certain affinity for soil particles, possibly due to its hydrophobic properties and its ability to interact with organic or mineral components in the soil matrix [12,13].

Table 3
Experimental conditions and kinetic model parameters.

Flubendiamide concentration/mg·L^{-1}	CMBC dosage/g	Adsorption efficiency/%	PFO			PSO		
			k_1/min^{-1}	q_e/mg·g^{-1}	R^2	k_2/g· mg^{-1}· min^{-1}	q_e/mg·g^{-1}	R^2
1.129	0	3.6	–	–	–	–	–	–
	0.02	62.44	0.048	0.316	0.901	0.164	0.772	0.994
	0.05	56.24	0.033	0.107	0.834	0.389	0.276	0.991
	0.1	50.40	0.040	0.078	0.975	0.515	0.132	0.989
1.257	0	4.2	–	–	–	–	–	–
	0.02	64.12	0.054	0.368	0.918	0.163	0.876	0.995
	0.05	58.47	0.052	0.192	0.978	0.319	0.327	0.995
	0.1	48.41	0.042	0.104	0.985	0.301	0.152	0.974
1.323	0	4.6	–	–	–	–	–	–
	0.02	68.03	0.050	0.317	0.936	0.221	0.950	0.998
	0.05	52.23	0.072	0.310	0.989	0.267	0.317	0.994
	0.1	45.50	0.056	0.156	0.970	0.196	0.166	0.949

Table 4
Adsorption isotherm parameters for flubendiamide adsorption on CMBC.

Adsorbent	Langmuir model			Freundlich model			RSS
	q_{max}/mg·g^{-1}	K_L/L·mg^{-1}	R^2	K_F/mg·g^{-1}·(L·mg^{-1})$^{1/n}$	$1/n$	R^2	
CMBC	−0.439	−1.437	0.981	5.897	0.401	0.998	2×10^{-4}

At 0.02 g of CMBC, as the flubendiamide concentration increased from 1.129 to 1.323 mg·L^{-1}, the adsorption efficiency increased gradually. The PFO model produced a lower R^2 value (0.901–0.936) than the PSO model (0.994–0.998), indicating that the adsorption of flubendiamide by 0.02 g of CMBC was driven primarily by chemical interactions. As the flubendiamide concentration was increased, k_2 remained stable and was almost the same at 1.129 and 1.257 mg·L^{-1}. However, k_2 increased with further addition up to 1.323 mg·L^{-1} flubendiamide. As the concentration of flubendiamide increased, the number of molecules exposed to the adsorption sites also increased, accelerating the mass transfer kinetics and increasing the adsorption rate [43,49]. In addition, the q_e values exhibited growth [50]. The highest recorded flubendiamide adsorption capacity of CMBC was 0.95 mg·g^{-1}.

At 0.05 g of CMBC, the adsorption efficiency increased slightly and then decreased gradually as the flubendiamide concentration increased. The adsorption process was described well by the PSO model (R^2 = 0.991–0.995). As flubendiamide concentration increased, k_2 values decreased gradually while q_e increased and then decreased slightly. The number of flubendiamide molecules surrounding the biochar increased, leading to competition between the molecules for binding to the adsorption sites. In addition, at low concentrations, more numerous flubendiamide molecules are available for adsorption, increasing q_e; however, when the concentration is too high, competition increases between the adsorption sites, decreasing q_e. This change from increasing to decreasing q_e indicates adsorption saturation [51].

At 0.1 g of CMBC, the adsorption efficiency decreased steadily with increasing flubendiamide concentration. The adsorption trend shifted gradually from being driven predominantly by chemical interactions to physical diffusion, as observed when comparing the R^2 values of the PFO and PSO models. The k_1 values increased slightly, while the k_2 values decreased greatly. The q_e values in both kinetic models gradually increased.

3.3. Adsorption isotherms

Table 4 presents the adsorption parameters of flubendiamide by CMBC according to the Langmuir and the Freundlich isotherm models. Although the Langmuir model has a suitable R^2, it does not fit the experimental data closely, as the negative parameters ($q_{max} < 0$ and $K_L < 0$) do not accurately reflect the physical nature of the adsorption process. On the contrary, the Freundlich model shows strong agreement with the experimental data, with a high coefficient of determination of R^2. This indicates that the Freundlich model can explain the adsorption process of flubendiamide by CMBC, and that the adsorption process is not homogeneous.

In the Freundlich model, the constant K_F indicates that CMBC is effective for flubendiamide adsorption. The value $1/n$ = 0.401 suggests that the adsorption is favorable and strong when the concentration of flubendiamide increases [12,52,53]. The 95% confidence intervals calculated for the Freundlich parameters indicate the degree of uncertainty associated with the model fit. For the evaluated adsorption data, the Freundlich constant K_F was found with a 95% confidence interval of [2.19, 15.89], while the exponent corresponds to an n value in the range [2.06, 3.19]. These results indicate that the Freundlich model provides a reasonable fit to the experimental data, while the calculated confidence intervals offer further insight into the reliability of the parameter estimates.

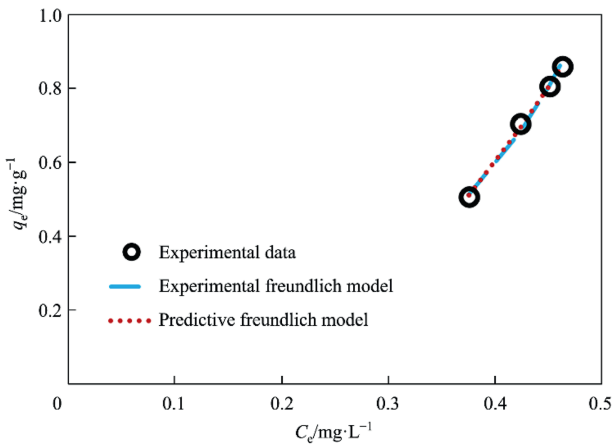

Fig. 7. Freundlich model for flubendiamide adsorption onto CMBC.

As shown in Fig. 7, results from the Freundlich model exhibit close agreement with experimental data. The predictive Freundlich model was also calculated from experimental data. The low RSS indicates a minimal discrepancy between experimental data and model prediction, demonstrating the model's high accuracy in describing the adsorption of flubendiamide by CMBC. In other words, the Freundlich model reflects the heterogeneity of the adsorption surface, suggesting that flubendiamide adsorption occurs with different adsorption sites on the CMBC surface.

4. Conclusions

We investigated the effectiveness of CMBC in reducing the load of flubendiamide in soil. First, we successfully synthesized CMBC in the presence of diverse functional groups. Experimental results showed that CMBC can adsorb flubendiamide at different concentrations across various doses. The highest adsorption efficiency was achieved when CMBC accounted for 1% (mass) of the contaminated soil, but further increases in the dose resulted in a decline in flubendiamide adsorption efficiency. The adsorption kinetics mainly followed the PSO model, with the adsorption mechanism primarily being a function of chemical interactions between flubendiamide and the functional groups on the CMBC surface. At 0.1 g of CMBC, as the flubendiamide concentration increased, the physical adsorption mechanism gradually became dominant. In addition, the experimental results of flubendiamide and CMBC correspond closely to the adsorption Freundlich isotherm. This suggests that adsorption occurs at different sites on the heterogeneous surface of CMBC. In this regard, the low RSS also confirms the accuracy of the Freundlich model. In summary, our study provides an overview of pesticides, flubendiamide in particular, and the kinetic and isotherm analyses of flubendiamide adsorption by CMBC, highlighting the potential application of modified biochar in environmental remediation.

CRediT Authorship Contribution Statement

Hong-Hue Thi Nguyen: Writing – original draft, Methodology, Investigation, Formal analysis, Data curation. Yong-Ho Choi: Validation, Software, Resources, Formal analysis. Yong-Hoon Jeong: Visualization, Software, Methodology. Jong-Guk Kim: Conceptualization, Data curation, Methodology, Supervision, Visualization. Dong-Heui Kwak: Writing – review & editing, Supervision, Project administration, Funding acquisition, Conceptualization.

Declaration of Competing Interest

The authors declare that they have no known competing financial interests or personal relationships that could have appeared to influence the work reported in this paper.

Acknowledgements

This paper was supported by research funds of Jeonbuk National University in 2024 and partly supported by the National Research Foundation of Korea (NRF-2019R1A2C1006441) from the Ministry of Education.

References

[1] D.J. Wang, N.B. Saleh, A. Byro, R. Zepp, E. Sahle-Demessie, T.P. Luxton, K.T. Ho, R.M. Burgess, M. Flury, J.C. White, C.M. Su, Nano-enabled pesticides for sustainable agriculture and global food security, *Nat. Nanotechnol.* 17 (4) (2022) 347–360.
[2] P. Kaushik, G. Kaushik, An assessment of structure and toxicity correlation in organochlorine pesticides, *J. Hazard. Mater.* 143 (1–2) (2007) 102–111.
[3] G. Twagirayezu, H.G. Cheng, Y.Y. Wu, H.Y. Lu, S.L. Huang, X. Fang, O. Irumva, Insights into the influences of biochar on the fate and transport of pesticides in the soil environment: a critical review, *Biochar* 6 (1) (2024) 9.
[4] J. Tae, K. Jo, R. Hee, Establishment of a GC-HRMS-IDMS-based modified QuEChERS approach for rapid, reliable, and simultaneous determination of organochlorine pesticides in soil, *Microchem. J.* 197 (2024) 109754.
[5] S. Medić Pap, B. Popović, N. Stojić, D. Danojević, M. Pucarević, J. Červenski, M. Šperanda, The environmental issue of pesticide residues in agricultural soils in Serbia, *Int. J. Environ. Sci. Technol.* 20 (7) (2023) 7263–7276.
[6] E.M. Asefa, Y.T. Damtew, J. Ober, Pesticide water pollution, human health risks, and regulatory evaluation: a nationwide analysis in Ethiopia, *J. Hazard. Mater.* 478 (2024) 135326.
[7] N. Dhankhar, J. Kumar, Impact of increasing pesticides and fertilizers on human health: a review, *Mater. Today Proc.* (2023), https://doi.org/10.1016/j.matpr.2023.03.766.
[8] S. Mitra, R.K. Saran, S. Srivastava, C. Rensing, Pesticides in the environment: degradation routes, pesticide transformation products and ecotoxicological considerations, *Sci. Total Environ.* 935 (2024) 173026.
[9] R. Kaur, D. Choudhary, S. Bali, S.S. Bandral, V. Singh, M.A. Ahmad, N. Rani, T.G. Singh, B. Chandrasekaran, Pesticides: an alarming detrimental to health and environment, *Sci. Total Environ.* 915 (2024) 170113.
[10] M. Tohnishi, T. Nishimatsu, K. Motoba, T. Hirooka, A. Seo, Development of a novel insecticide, flubendiamide, *J. Pestic. Sci.* 35 (4) (2010) 508–515.
[11] M. Tohnishi, H. Nakao, T. Furuya, A. Seo, H. Kodama, K. Tsubata, S. Fujioka, H. Kodama, T. Hirooka, T. Nishimatsu, Flubendiamide, a novel insecticide highly active against lepidopterous insect pests, *J. Pestic. Sci.* 30 (4) (2005) 354–360.
[12] S.K. Das, I. Mukherjee, A. Kumar, Effect of soil type and organic manure on adsorption-desorption of flubendiamide, *Environ. Monit. Assess.* 187 (7) (2015) 403.
[13] S.K. Das, I. Mukherjee, Effect of light and pH on persistence of flubendiamide, *Bull. Environ. Contam. Toxicol.* 87 (3) (2011) 292–296.
[14] S.K. Das, I. Mukherjee, Effect of moisture and organic manure on persistence of flubendiamide in soil, *Bull. Environ. Contam. Toxicol.* 88 (4) (2012) 515–520.
[15] A.P. Khedulkar, B. Pandit, V.D. Dang, R.A. Doong, Agricultural waste to real worth biochar as a sustainable material for supercapacitor, *Sci. Total Environ.* 869 (2023) 161441.
[16] D.M. Saharudin, H.K. Jeswani, A. Azapagic, Biochar from agricultural wastes: environmental sustainability, economic viability and the potential as a negative emissions technology in Malaysia, *Sci. Total Environ.* 919 (2024) 170266.
[17] K. Ramesh, V. Raghavan, Agricultural waste-derived biochar-based nitrogenous fertilizer for slow-release applications, *ACS Omega* 9 (4) (2024) 4377–4385.
[18] Y.F. Ma, J.Y. Tang, S.Y. Chen, L. Yang, S.T. Shen, X. Chen, Z.L. Zhang, Ball milling and acetic acid co-modified sludge biochar enhanced by electrochemistry to activate peroxymonosulfate for sustainable degradation of environmental concentration neonicotinoids, *J. Hazard. Mater.* 444 (Pt A) (2023) 130336.
[19] X. Dong, Y. Chu, Z. Tong, M.N. Sun, D.D. Meng, X.T. Yi, T.C. Gao, M.H. Wang, J. S. Duan, Mechanisms of adsorption and functionalization of biochar for pesticides: a review, *Ecotoxicol. Environ. Saf.* 272 (2024) 116019.
[20] T.G. Ambaye, A. Hassani, M. Vaccari, A. Franzetti, S. Prasad, F. Formicola, A. Rosatelli, M.Z.U. Rehman, G. Mohanakrishna, S.V. Ganachari, T.M. Aminabhavi, S. Rtimi, Emerging technologies for the removal of pesticides from contaminated soils and their reuse in agriculture, *Chemosphere* 362 (2024) 142433.
[21] H.H.T. Nguyen, H.M. Nguyen, T.M. Tran-Thuy, L.Q. Nguyen, H.H. Lam, D.V. Nguyen, One-pot preparation of magnetic biochar from dragon fruit branch for catalytic ozonation of sunset yellow, *Rasayan J. Chem.* 16 (3) (2023) 1229–1237.
[22] X.L. Liao, S.X. Mao, Y.X. Shan, W.R. Gao, S.S. Wang, S. Malghani, Impact of iron-modified biochars on soil nitrous oxide emissions: variations with iron salts and soil fertility, *J. Environ. Manag.* 356 (2024) 120571.
[23] H. Samaraweera, A. Rivera, K. Carter, T. Felder, S. Nawalage, I. Chui, F. Perez, A.H. Khan, T. Mlsna, Green iron oxide-modified biochar for methylene blue removal from aqueous solutions, *Groundw. Sustain. Dev.* 21 (2023) 100945.
[24] H.M. Nguyen, T.B. Truong, H.T. Nguyen, P.T. Tran, T.M. Tran-Thuy, L.Q. Nguyen, D.V. Nguyen, Catalytic ozonation of ponceau 4R using multifunctional magnetic biochar prepared from rubber seed shell, *J. Ecol. Eng.* 24 (12) (2023) 143–151.
[25] S. Lee, L.T. Hao, J. Park, D.X. Oh, D.S. Hwang, Nanochitin and nanochitosan: chitin nanostructure engineering with multiscale properties for biomedical and environmental applications, *Adv. Mater.* 35 (4) (2023) e2203325.
[26] Y.B. Yu, W.T. Liu, Y.N. Zhang, B.L. Zhang, Y.P. Jin, S.J. Chen, S.S. Tang, Y.J. Su, X. X. Yu, G. Chen, Chitosan/magnetic biochar composite with enhanced reusability: synergistic effect of functional groups and multilayer structure, *Arab. J. Chem.* 17 (5) (2024) 105746.
[27] N. Gao, W.Z. Du, M.Y. Zhang, G.X. Ling, P. Zhang, Chitosan-modified biochar: preparation, modifications, mechanisms and applications, *Int. J. Biol. Macromol.* 209 (Pt A) (2022) 31–49.
[28] H.T. Nguyen, Y.H. Choi, E.B. Kim, Y.H. Jeong, J.W. Lee, K.H. Park, Y.J. Woo, S. Ameen, D.H. Kwak, Investigation of Pb(II) adsorption by amine group

enriched chitosan encapsulated iron oxides doped biochar for soil remediation, *Carbon Trends* 19 (2025) 100465.
[29] S.I. Suh, I.S. Hwang, H.S. Lee, S.J. Ki, M.H. Son, Development and application of an advanced algorithm for environmental risk assessment and safety management of pesticide residues in agricultural soils: monitoring of currently used pesticide in upland soils, *Environ. Int.* 190 (2024) 108865.
[30] H.G. Cheng, D. Xing, S. Lin, Z.X. Deng, X. Wang, W.J. Ning, P.W. Hill, D.R. Chadwick, D.L. Jones, Iron-modified biochar strengthens simazine adsorption and decreases simazine decomposition in the soil, *Front. Microbiol.* 13 (2022) 901658.
[31] J.Y. Nie, Z.K. Wang, Q.L. Hu, Difference between chitosan hydrogels *via* alkaline and acidic solvent systems, *Sci. Rep.* 6 (2016) 36053.
[32] M. Gopal, E. Mishra, Analytical method for estimation of a new insecticide flubendiamide and its safety evaluation for usage in rice crop, *Bull. Environ. Contam. Toxicol.* 81 (4) (2008) 360–364.
[33] N.Đ. Phương, Đ.T.M. Phượng, N.H. Chiếm, P.N. Thoa, N.X. Lộc, Nitrate adsorption by biochar produced from rice husk (o. sativa L., OM5451), *Hue Univ. J. Sci. Nat. Sci.* 130 (1A) (2021) 31–39.
[34] N.F. Al-Harby, E.F. Albahly, N.A. Mohamed, Kinetics, isotherm and thermodynamic studies for efficient adsorption of Congo red dye from aqueous solution onto novel cyanoguanidine-modified chitosan adsorbent, *Polymers* 13 (24) (2021) 4446.
[35] S. Chen, C.X. Qin, T. Wang, F.Y. Chen, X.L. Li, H.B. Hou, M. Zhou, Study on the adsorption of dyestuffs with different properties by sludge-rice husk biochar: adsorption capacity, isotherm, kinetic, thermodynamics and mechanism, *J. Mol. Liq.* 285 (2019) 62–74.
[36] K.S.W. Sing, Reporting physisorption data for gas/solid systems with special reference to the determination of surface area and porosity (recommendations 1984), *Pure Appl. Chem.* 57 (4) (1985) 603–619.
[37] L.F. Xu, J.C. Zhang, J.H. Ding, T. Liu, G. Shi, X.Q. Li, W. Dang, Y.S. Cheng, R.B. Guo, Pore structure and fractal characteristics of different shale lithofacies in the dalong formation in the western area of the Lower Yangtze platform, *Minerals* 10 (1) (2020) 72.
[38] H.S. Lee, H.S. Shin, Competitive adsorption of heavy metals onto modified biochars: comparison of biochar properties and modification methods, *J. Environ. Manag.* 299 (2021) 113651.
[39] K.X. Wang, H. Ma, S.Y. Pu, C. Yan, M.T. Wang, J. Yu, X.K. Wang, W. Chu, A. Zinchenko, Hybrid porous magnetic bentonite-chitosan beads for selective removal of radioactive cesium in water, *J. Hazard. Mater.* 362 (2019) 160–169.
[40] S.B. Liu, B.Y. Huang, L.Y. Chai, Y.G. Liu, G.M. Zeng, X. Wang, W. Zeng, M.R. Shang, J.Q. Deng, Z. Zhou, Enhancement of As(V) adsorption from aqueous solution by a magnetic chitosan/biochar composite, *RSC Adv.* 7 (18) (2017) 10891–10900.
[41] N. Bombuwala Dewage, R.E. Fowler, C.U. Pittman Jr., D. Mohan, T. Mlsna, Lead (Pb^{2+}) sorptive removal using chitosan-modified biochar: batch and fixed-bed studies, *RSC Adv.* 8 (45) (2018) 25368–25377.
[42] N.X. Loc, P.T.T. Tuyen, L.C. Mai, D.T.M. Phuong, Chitosan-modified biochar and unmodified biochar for methyl orange: adsorption characteristics and mechanism exploration, *Toxics* 10 (9) (2022) 500.
[43] H. Deveci, Y. Kar, Adsorption of hexavalent chromium from aqueous solutions by bio-chars obtained during biomass pyrolysis, *J. Ind. Eng. Chem.* 19 (1) (2013) 190–196.
[44] T. Chen, Z.Y. Zhou, R. Han, R.H. Meng, H.T. Wang, W.J. Lu, Adsorption of cadmium by biochar derived from municipal sewage sludge: impact factors and adsorption mechanism, *Chemosphere* 134 (2015) 286–293.
[45] D. Kołodyńska, R. Wnętrzak, J.J. Leahy, M.H.B. Hayes, W. Kwapiński, Z. Hubicki, Kinetic and adsorptive characterization of biochar in metal ions removal, *Chem. Eng. J.* 197 (2012) 295–305.
[46] M. Kılıç, Ç. Kırbıyık, Ö. Çepelioğullar, A.E. Pütün, Adsorption of heavy metal ions from aqueous solutions by bio-char, a by-product of pyrolysis, *Appl. Surf. Sci.* 283 (2013) 856–862.
[47] N. Ertugay, Y.K. Bayhan, Biosorption of Cr (VI) from aqueous solutions by biomass of Agaricus bisporus, *J. Hazard. Mater.* 154 (1–3) (2008) 432–439.
[48] G. Dönmez, Z. Aksu, Removal of chromium(VI) from saline wastewaters by *Dunaliella* species, *Process. Biochem.* 38 (5) (2002) 751–762.
[49] Z. Aksu, Equilibrium and kinetic modelling of cadmium(II) biosorption by C. vulgaris in a batch system: effect of temperature, *Sep. Purif. Technol.* 21 (3) (2001) 285–294.
[50] H.H. Zhang, W.Z. Zhong, R.B. Qiu, L.J. Han, Kinetics and modeling of Pb (II) adsorption in pellet biochar based on micro-computed tomography characterization, *Bioresour. Technol.* 387 (2023) 129645.
[51] G.J. Cai, Z.L. Ye, Concentration-dependent adsorption behaviors and mechanisms for ammonium and phosphate removal by optimized Mg-impregnated biochar, *J. Clean. Prod.* 349 (2022) 131453.
[52] P.P. Wang, X.G. Liu, X.H. Wu, J. Xu, F.S. Dong, Y.Q. Zheng, Evaluation of biochars in reducing the bioavailability of flubendiamide in water/sediment using passive sampling with polyoxymethylene, *J. Hazard. Mater.* 344 (2018) 1000–1006.
[53] S.K. Das, I. Mukherjee, Low cost biomass derived biochar amendment on persistence and sorption behaviour of flubendiamide in soil, *Bull. Environ. Contam. Toxicol.* 105 (2) (2020) 261–269.